Supplementary Information

Diphenylphosphine oxide decorated multi-resonance TADF emitter for narrowband green electroluminescence with EQE of 32.4%

Junjie Dong, Yulin Xu, Shuni Wang, Jingsheng Miao, Nengquan Li, Zhongyan Huang*, Chuluo Yang

Shenzhen Key Laboratory of New Information Display and Storage Materials, College of Materials Science and Engineering, Shenzhen University, Shenzhen 518060, People's Republic of China

Corresponding Author:
Zhongyan Huang, E-mail: zyhuang@szu.edu.cn

General information

Quantum Chemical Calculations: quantum chemical calculations were performed by the Gaussian 09 program package, density functional theory (DFT) using the B3LYP/6-31G(d) was performed for achieved optimized molecular geometries. Based on the optimized geometric configurations, the dihedral angles of these molecules and the highest occupied molecular orbital (HOMO), as well as the lowest unoccupied molecular orbital (LUMO) were obtained logically. The time-dependent density functional theory (TD-DFT) calculations were performed at the B3LYP/6-31G(d) level. The calculated UV-vis spectra were performed at the M062X functional.

Photophysical Characterization: Shimadzu UV-2700 spectrophotometer (Shimadzu, Japan) was applied to record UV-vis spectra at 25 ^{o}C. Photoluminescence (PL) spectra were determined on a Hitachi F-7100 fluorescence spectrophotometer (Hitachi, Japan) at 25 ^{o}C or 77 K. The transient PL decay curves were obtained by FluoTime 300 (PicoQuant GmbH) with a Picosecond Pulsed UV-LASTER (LASTER375) as the excitation source. The photoluminescence quantum yields (Φ_{PLQYs}) were achieved by a Hamamatsu UV-NIR absolute PL quantum yield spectrometer (C13534, Hamamatsu Photonics) equipped with a calibrated integrating sphere, the integrating sphere was purged with dry argon to maintain an inert atmosphere.

Thermal Characterization: A TGA 55 (TA instrument) thermal analysis system was employed to analyze thermal gravimetric analysis (TGA) ranging from 25 °C to 800 °C with a heating rate of 10 K min^{-1} under nitrogen flushing. Differential scanning calorimetry (DSC) was measured from 50 °C to 350 °C on a Q200 (TA instrument) with a 10 K min^{-1} heating rate under nitrogen flushing.

Electrochemical Characterization: Cyclic voltammograms (CV) were obtained in dichloromethane at room temperature with a CHI600 electrochemical workstation at 25 ^{o}C and a scan speed of 50 mV s^{-1}. The electrochemical oxidation potentials were collected by cyclic voltammetry measurements via a CHI660 electrochemical workstation (Chenhua, China) and ferroceniumferrocene (Fc/Fc^+) was used as the internal reference, tetrabutylammonium hexafluorophosphate (0.1 M) was used as the supporting electrolyte. A platinum plate electrode was utilized as the working electrode, a platinum wire was utilized as the counter electrode and Ag/AgCl as reference electrode.

Analysis of Rate Constants: The rate constants of radiative decay ($k_{r,S}$) and nonradiative decay ($k_{nr,S}$) from S_1 to S_0 states, the rate constants of intersystem crossing (k_{ISC}) and reverse intersystem crossing (k_{RISC}) were calculated from the following six equations:

$k_p = 1/\tau_p$……………………………………………………………Eq.(1)

$k_d = 1/\tau_d$……………………………………………………………Eq.(2)

$k_{r,S} = \Phi_p k_p + \Phi_d k_d \approx \Phi_p k_p$…………………………… ………………Eq.(3)

$k_{nr,S} = \frac{1 - \Phi_{PL}}{\Phi_{PL}} k_{r,S}$ ……………………………………………………………Eq.(4)

$k_{ISC} = k_p - k_{r,S} - k_{nr,S}$……………………………………………………Eq.(5)

$k_{RISC} = (k_p k_d \Phi_d)/(k_{ISC}\Phi_p)$……………………………………………Eq.(6)

The τ_p and τ_d represent the prompt and decay fluorescence lifetime, which determined from transient PL spectra. The k_p and k_d represent the decay rate constants for prompt and delayed fluorescence, respectively. Φ_p and Φ_d indicate prompt and delayed fluorescence components and can be distinguished from the total Φ_{PL} by comparing the integrated intensities of prompt and delayed components in the transient PL spectra.

Device Fabrication and Measurement: To evaluate the EL performance of PhCzBN-PO as emitter, we fabricated multilayered TADF OLEDs. The ITO coated glass substrates with a sheet resistance of 15 Ω $square^{-1}$ were ultrasonic cleaned with acetone/ethanol and dried with nitrogen gas flow, followed by 20 min ultraviolet light-ozone (UVO) treatment in a UV-ozone surface processor (PL16 series, Sen Lights Corporation). Then the sample was transferred to the deposition system. All organic layers were deposited at a rate of 1 Å s^{-1}, and subsequently Liq was deposited at 0.2 Å s^{-1} and then capped with Al (ca. 4 Å s^{-1}) through a shadow mask in a vacuum of 2×10^{-5} mbar. For all the devices, the emitting areas were determined by the overlap of two electrodes as 0.09 cm^2. The as-fabricated devices were measured in ambient environment without any encapsulation. The EL spectra and Commission Internationale de l'Eclairage (CIE) coordinates were recorded with a Keithley 2400 source meter unit. The current density-voltage-luminance (J-V-L) curves of the devices were measured with a PHOTO RESEARCH SpectraScan PR 735 spectrometer. The EQE was calculated from the current density, luminance and EL (electroluminescence) spectrum, assuming a Lambertian distribution.

Synthesis and Characterization

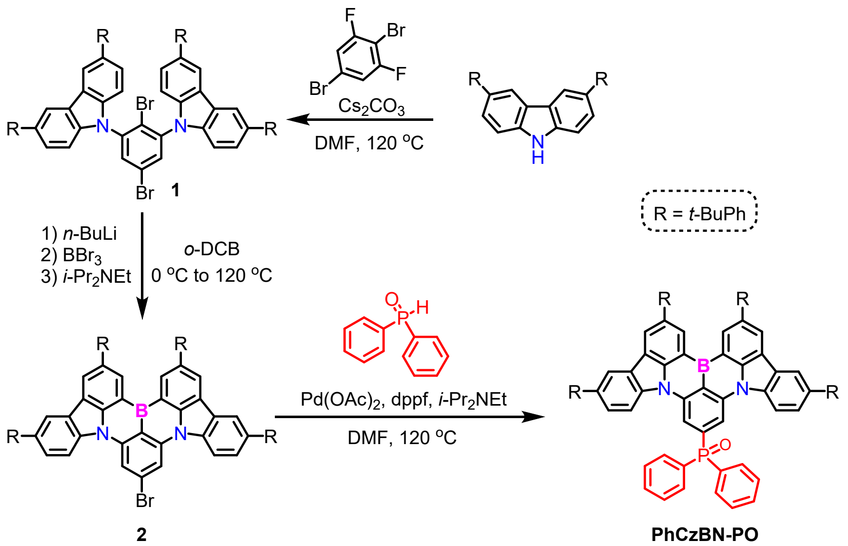

synthesis of 1**:** To a mixture of 3,6-bis(4-(*tert*-butyl)phenyl)-9*H*-carbazole (1.91 g, 6 mmol) and Cesium carbonate (Cs_2CO_3) (1.96 g, 6 mmol) in 20 mL DMF, 2,5-dibromo-1,3-difluorobenzene (0.54 g, 2 mmol) was added under argon atmosphere, then the reaction was stirred at 120 °C for 12 h. After cooling to room temperature, the mixture was diluted with dichloromethane and washed with water for three times. Then the diluted solvent was dried over sodium sulfate (Na_2SO_4) for 15 min and removed by rotatory evaporation. The crude product was purified by column chromatography, resulting in a white solid (1.7 g, 78%). ^{1}H NMR (400 MHz, $CDCl_3$) δ (ppm): 8.42 (d, J = 1.6 Hz, 4H), 7.93 (s, 2H), 7.78 (dd, J = 8.4, 1.6 Hz, 4H), 7.73-7.68 (m, 8H), 7.57-7.53 (m, 8H), 7.33 (d, J = 8.4 Hz, 4H), 1.43 (s, 36H).

synthesis of 2**:** Under argon atmosphere, 1.6 M *n*-BuLi (0.66 mL, 1.75 mmol) in *n*-hexane was added slowly to a solution of intermediate **1** (1.64 g, 1.5 mmol) in 1,2-dichlorobenzene (20 mL) at 0 °C. After stirring at room temperature for 2 h, boron tribromide (0.3 mL, 3.0 mmol) was added at 0 °C, then the reaction was stirred at room temperature for 1 h. After *N*,*N*-diisopropylethylamine (*i*-Pr$_2$NEt) (0.51 mL, 3.0 mmol) was added at 0 °C, the reaction mixture was allowed to stir at room temperature for 0.5 h. After heating to 160 °C for 12 h, the reaction mixture was cooled to room temperature and then 2.0 mL *i*-Pr_2NEt was added to the mixture. The mixture was diluted with dichloromethane and washed with water for 3 times. The organic solvent was dried over Na_2SO_4 for 15 min and removed by rotatory evaporation. Then the mixture was dissolved by dichloromethane and then methanol was added in solution until a large amount of solid precipitate. The mixture was filtered and the solid was washed by methanol, then dried by vacuum to give the intermediate **2** as orange solid (1.31 g, 85%). The intermediate **2** was directly used to the next step.

***synthesis of PhCzBN-PO*:** Under argon atmosphere, diphenylphosphine oxide (250 mg, 1.2 mmol), *i*-Pr_2NEt (0.15 mL, 1.5 mmol), palladium acetate ($Pd(OAc)_2$) (11 mg, 0.05 mmol), and 1,1'-Bis(diphenylphosphino)ferrocene (dppf) (50 mg, 0.10 mmol), was added to a solution of intermediate **2** (1.0 g, 1.0 mmol) in DMF (20 mL). After heating to 120 ^{o}C for 8 h, the reaction mixture was cooled to room temperature. The mixture was diluted with dichloromethane and washed with water for 3 times. Then the diluted solvent was dried over Na_2SO_4 for 15 min and removed by rotatory evaporation. The crude product was purified by column chromatography, resulting in orange solid (350 mg, 30%). ^{1}H NMR (500 MHz, $CDCl_3$) δ (ppm): 9.02 (s, 2H), 8.43 (s, 2H), 8.42 (s, 1H), 8.40 (s, 1H), 8.24 (s, 2H), 7.87 (d, J = 7.5 Hz, 2H), 7.85 (d, J = 7.5 Hz, 2H), 7.77 (d, J = 8.0 Hz, 2H), 7.75 (d, J = 8.0 Hz, 4H), 7.67-7.64 (m, 6H), 7.58-7.50 (m, 14H), 1.45 (s, 18H), 1.43 (s, 18H). ^{13}C NMR (126 MHz, $CDCl_3$) δ (ppm): 150.21, 149.95, 143.47, 143.35, 142.16, 138.85, 138.81, 137.93, 135.60, 135.49, 132.53, 132.46, 132.27, 131.90, 131.81, 128.94, 128.84, 127.41, 127.32, 126.90, 126.01, 125.95, 125.91, 124.19, 122.80, 122.07, 118.97, 114.81, 111.45, 111.36, 34.63, 31.53, 31.49. HRMS (ESI^{+}): calcd for $[C_{82}H_{74}BN_2OP+H]^{+}$, 1145.5710; found 1145.5740. Elemental analysis calcd. (%) for $C_{82}H_{74}BN_2OP$: C, 86.00; N, 2.45; H, 6.51; found: C, 84.6; N, 2.67; H, 5.66.

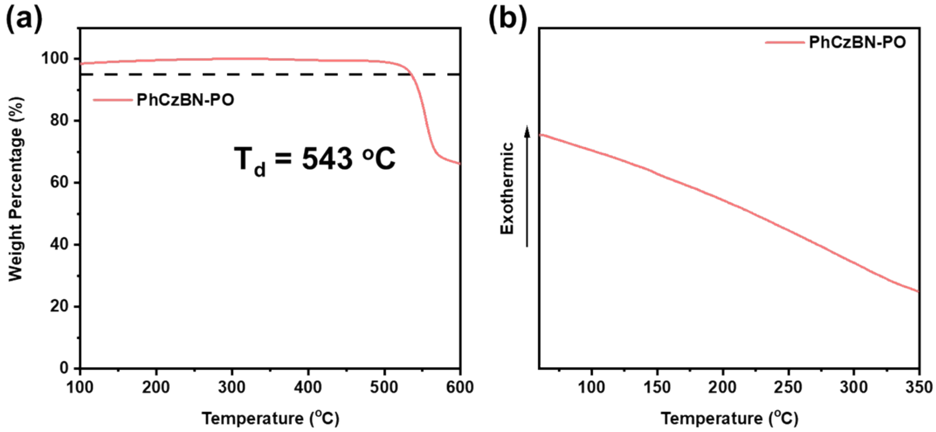

Figure S1. The (a) TGA and (b) DSC curves of **PhCzBN-PO**.

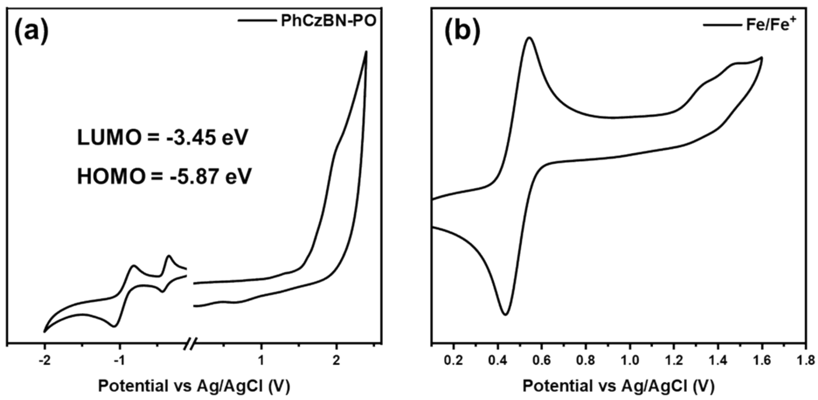

Figure S2. The cyclic voltammetry curves of (a) **PhCzBN-PO** and (b) ferrocene.

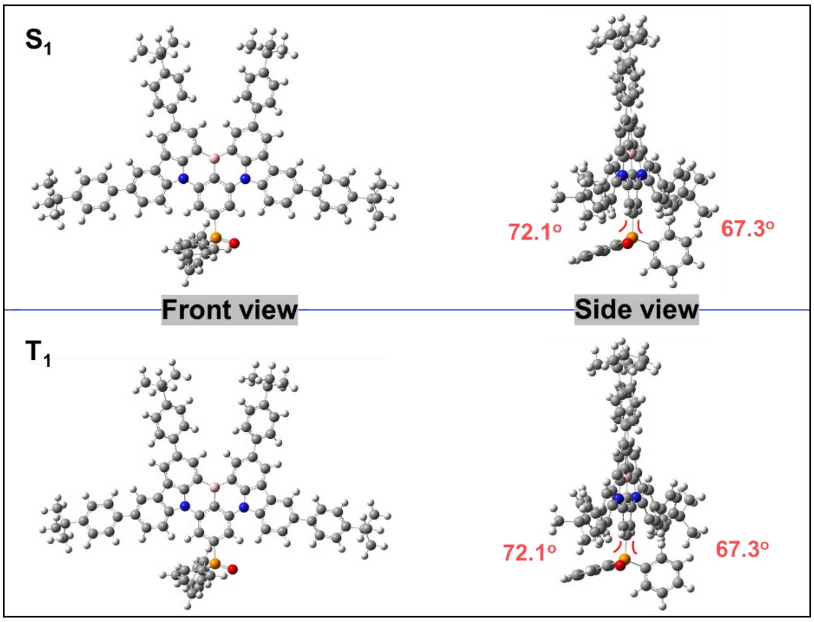

Figure S3. The optimized geometry and dihedral angles of **PhCzBN-PO** at the S_1 and T_1 states.

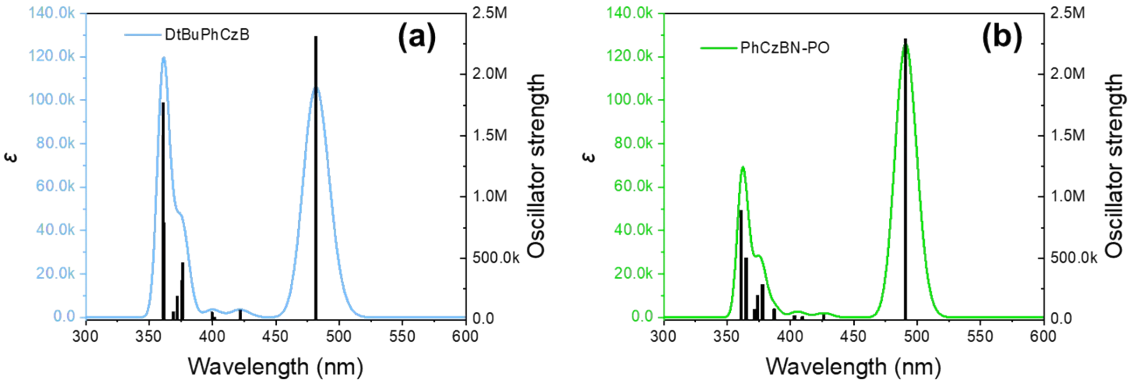

Figure S4. Calculated UV-vis spectra of **DtBuPhCzB** and **PhCzBN-PO**. The calculated spectra (with n state = 10) were shifted by 0.62 eV towards lower energies, and the major transition of calculation align well with the experimental data.

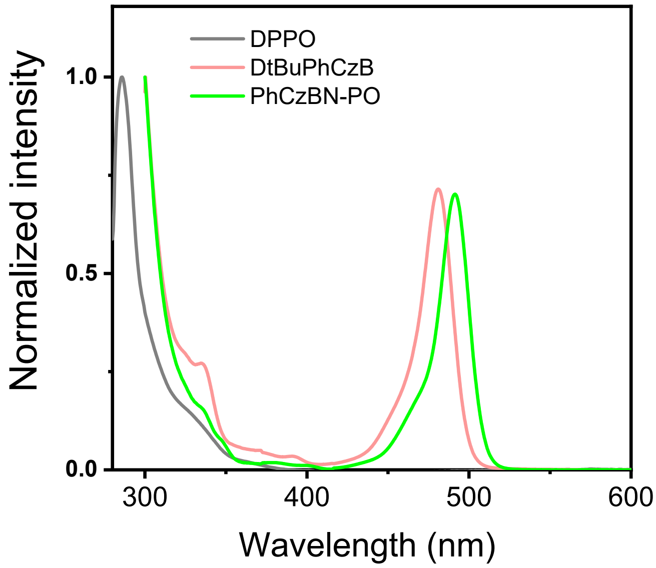

Figure S5. The UV-vis absorption spectra of **DPPO**, **DtBuPhCzB** and **PhCzBN-PO** in dilute toluene (10^{-5} M) solutions.

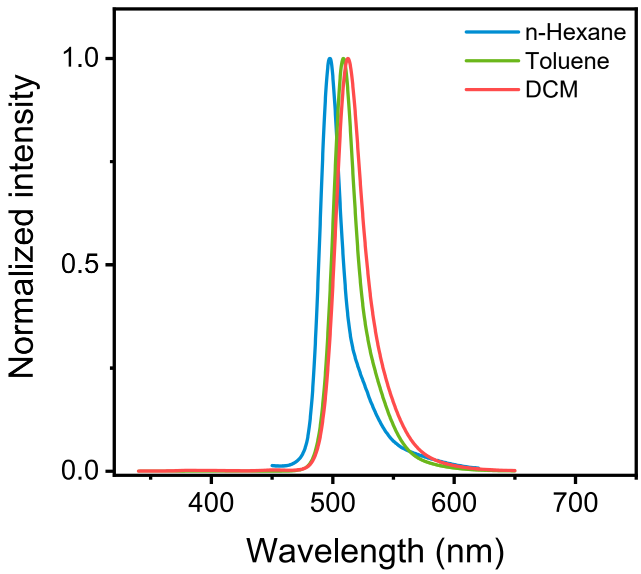

Figure S6. Solvatochromic effect on the PL spectra with excitation wavelength at 360 nm in different solvents at concentration of 1×10^{-5} M of **PhCzBN-PO**.

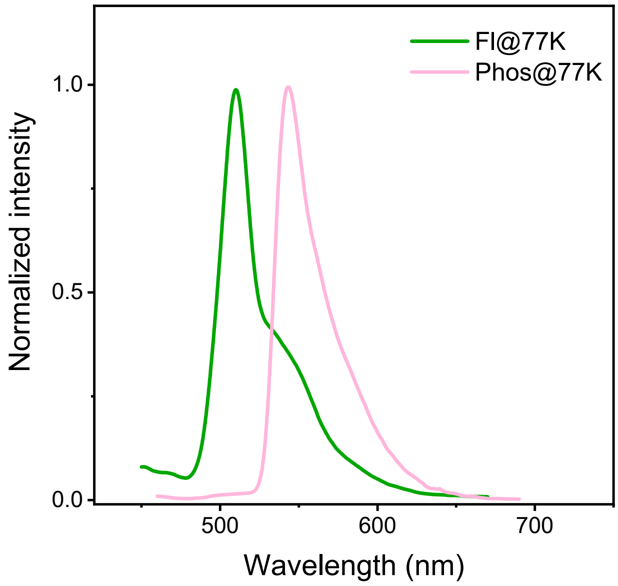

Figure S7. The fluorescence and phosphorescence (measured at 77 K) spectra of **PhCzBN-PO** in toluene solution.

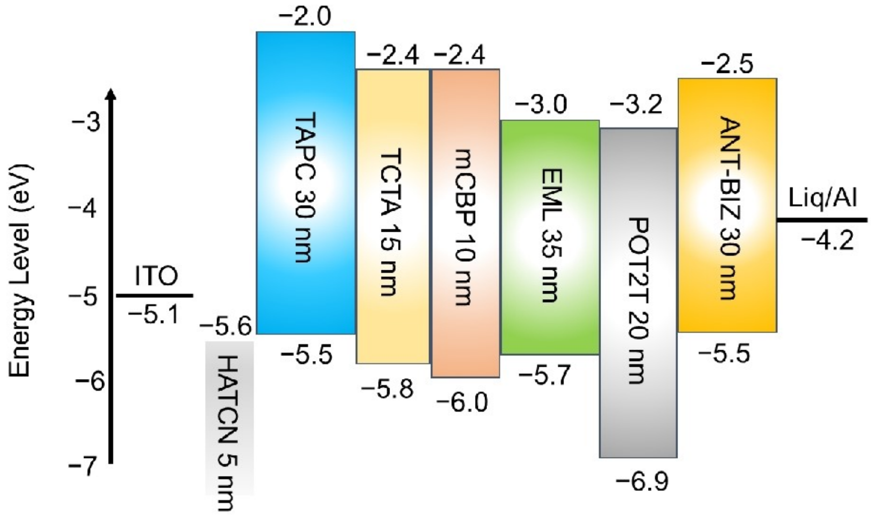

Figure S8. Device architecture for the MR-TADF OLEDs with energy levels of each layer material.

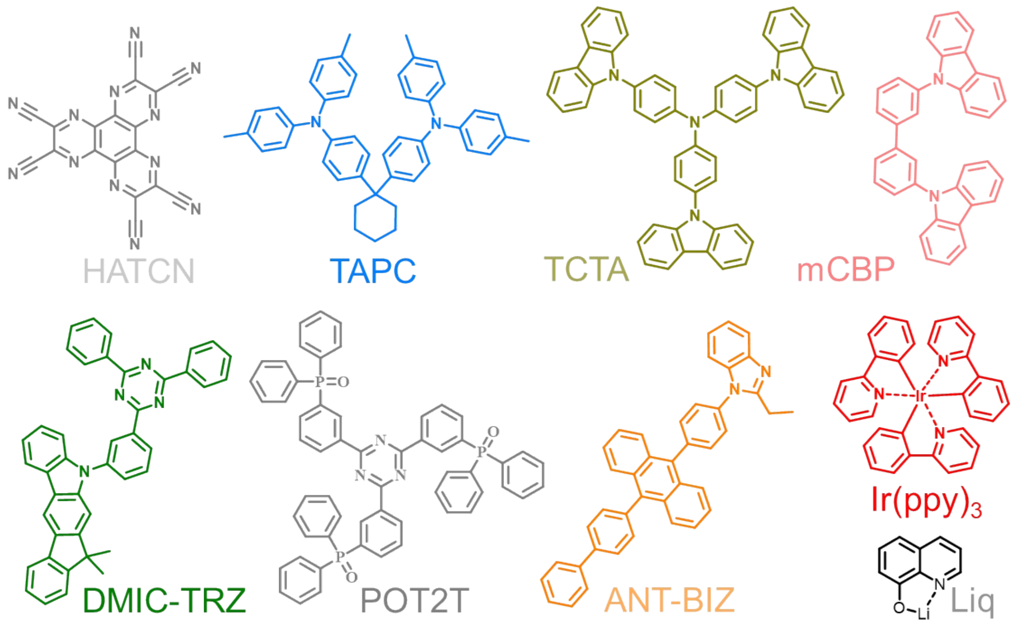

Figure S9. Molecular structures of relevant materials employed in devices.

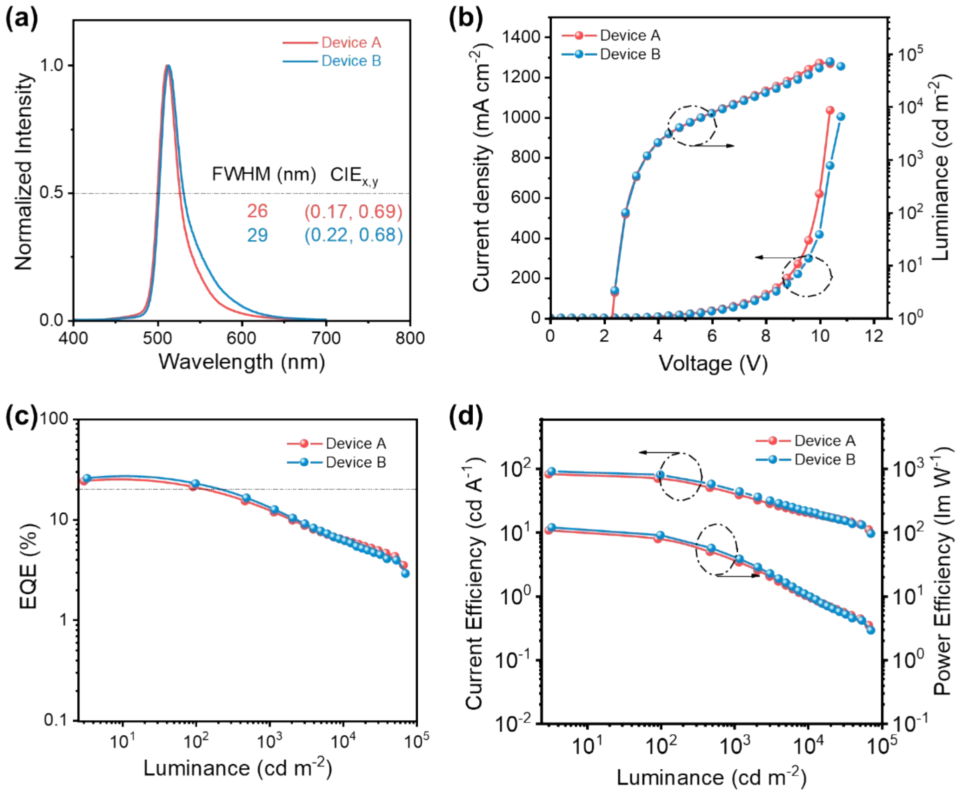

Figure S10. EL performance. (a) EL spectrum, (b) current density and luminance versus voltage characteristics, (c) EQE-luminance curves, (d) current efficiency and power efficiency versus luminance characteristics of the device A and B.

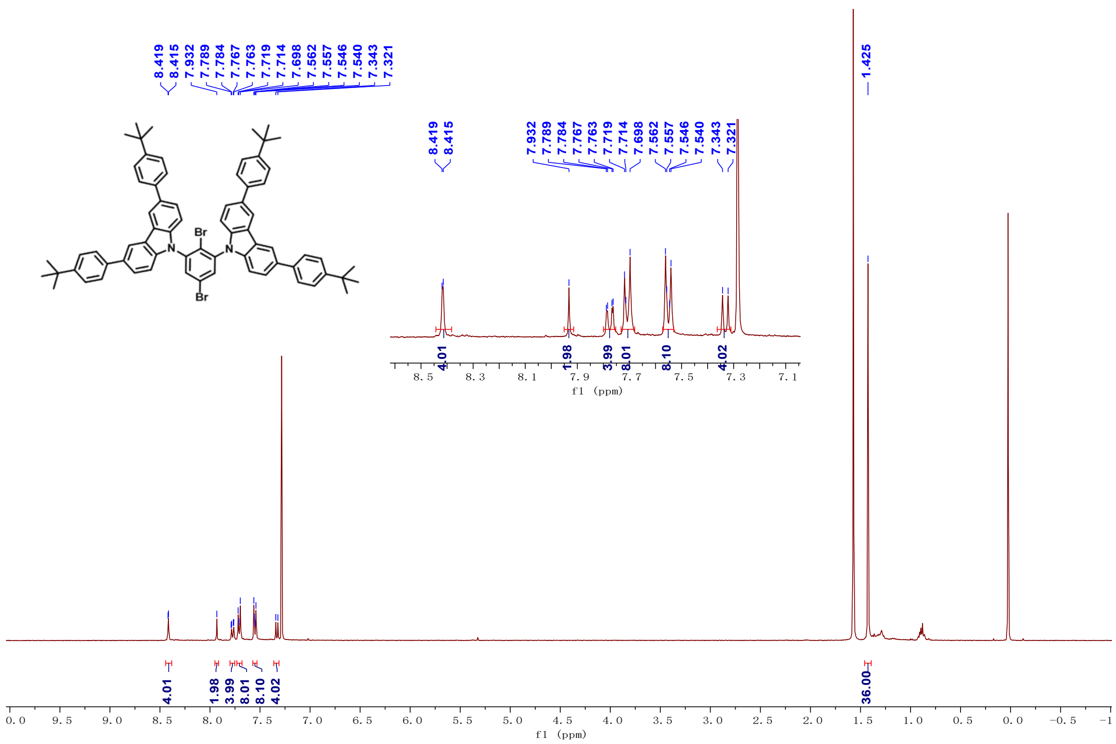

Figure S11. ^{1}H NMR spectrum of **1**.

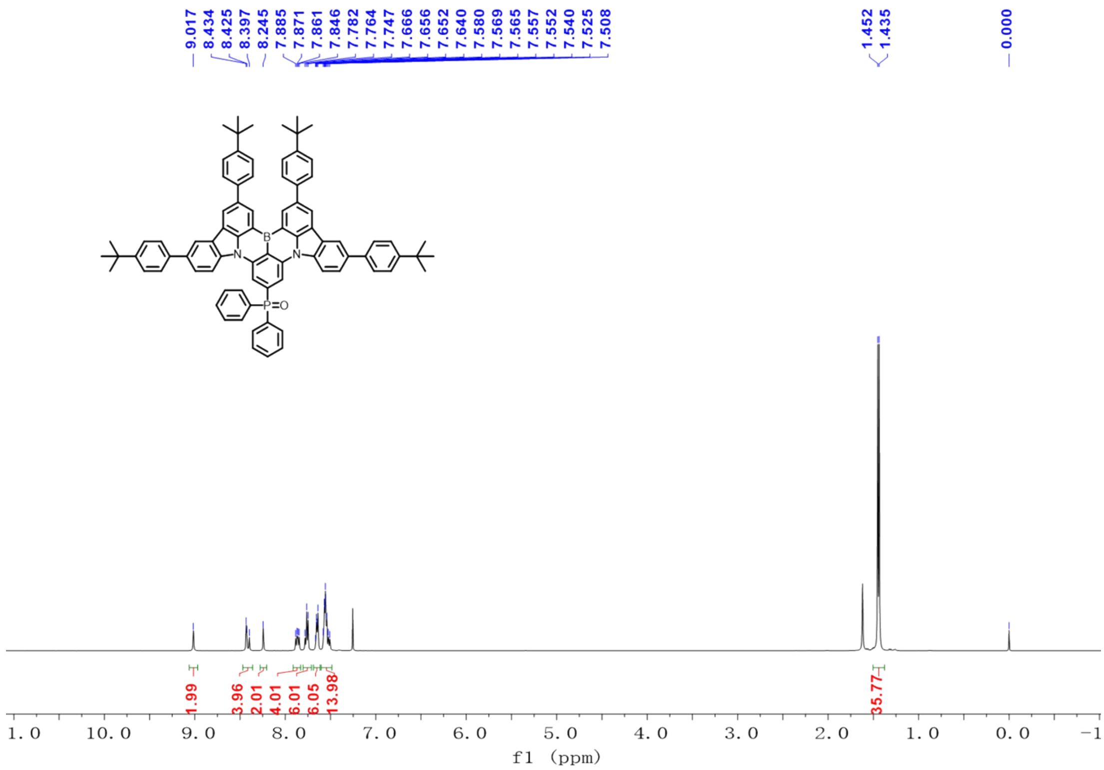

Figure S12. ^{1}H NMR spectrum of **PhCzBN-PO**.

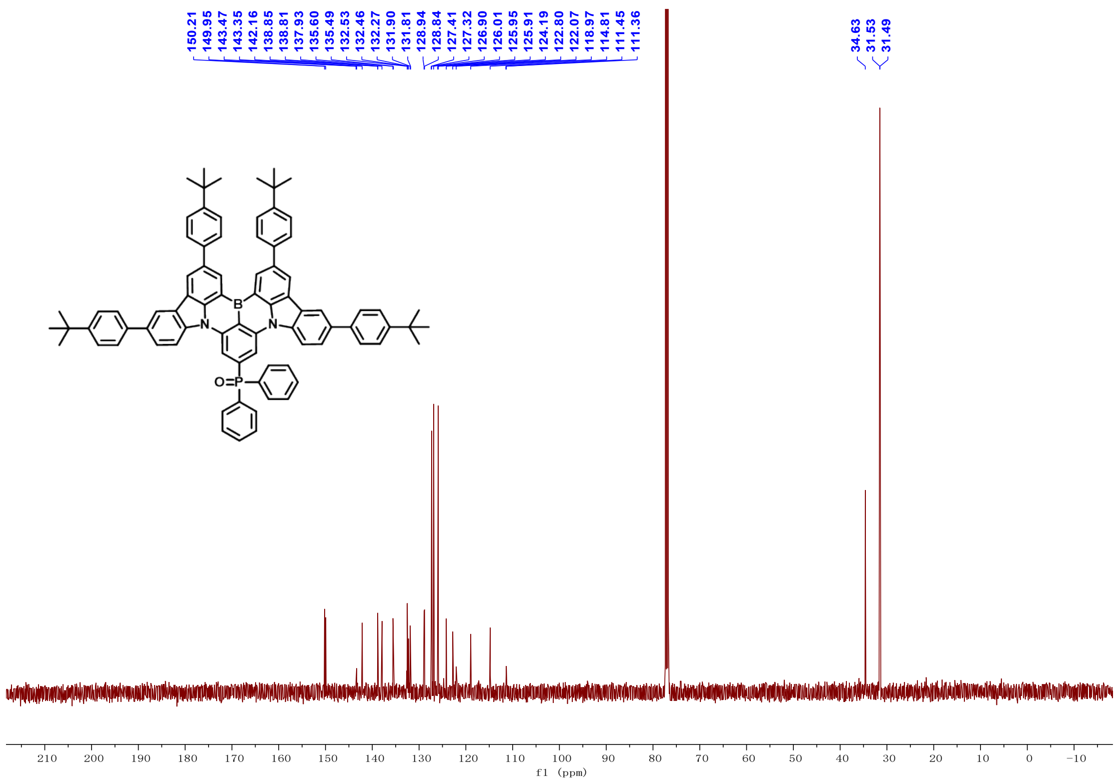

Figure S13. ^{13}C NMR spectrum of **PhCzBN-PO**.

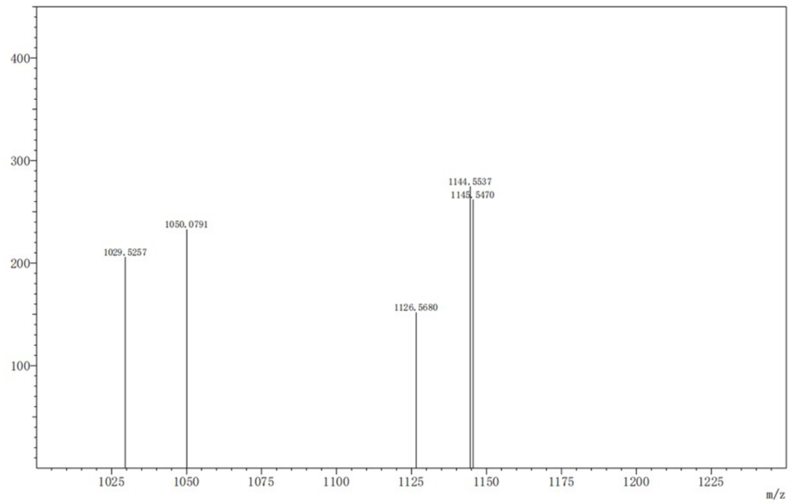

Figure S14. HR-MS spectrum of **PhCzBN-PO**.

Table S1. EL performances of reported MR emitters containing DPPO group.

Emitter	EL_{peak} [nm]	FWHM [nm]	$EQE_{max/1000}$ [%]	CIE [x,y]	Ref.
PhCzBN-PO	513	29	32.4/31.4	0.24, 0.67	**This work**
DPPO-BN	498	30	31.3/21.7	0.11, 0.52	*Chem. Eng. J.* **2024**, *489*, 151517
TPPO-BN	508	41	39.8/31.9	0.17, 0.64	*Chem. Eng. J.* **2024**, *489*, 151517
***o*-BNPO**	496	26	36.0/14.8	0.09, 0.48	*Adv. Funct. Mater.* **2024**, 2313726
CzP2PO	379	34	8.0/8.0	0.15, 0.04	*Angew. Chem. Int. Ed.* **2024**, *63,* e202316479
tBCzP2PO	384	32	15.1/14.7	0.14, 0.04	*Angew. Chem. Int. Ed.* **2024**, *63,* e202316479
tCBNDASPO	472	32	28.0/15.3	0.12, 0.17	*Research.* **2022**;2022
tCBNDADPO	472	28	30.8/16.2	0.14,0.22	*Adv. Mater.* **2022**, *34,* 2110547
TPPO-tBu-DiKTa	480	46	24.4/3.6	0.13, 0.32	*Aggregate.* **2024,** e571.
pICz-PPO	442	27	12.1/-	0.16, 0.08	*J. Mater. Chem. C,* **2024**, *12,* 2485
pICz-2PPO	441	24	17.7/-	0.16, 0.07	*J. Mater. Chem. C,* **2024**, *12,* 2485